ACS OMEGA

Open Access

http://pubs.acs.org/journal/acsodf

Article

Preparation and Characterization of Carboxymethyl Chitosan/Sodium Alginate Composite Hydrogel Scaffolds Carrying Chlorhexidine and Strontium-Doped Hydroxyapatite

Zijian Liu, Shangbo Li, Zexian Xu, Li Li, Yanshan Liu, Xiaohan Gao, Yaru Diao, Liqiang Chen,* and Jian Sun*

Cite This: *ACS Omega* 2024, 9, 22230−22239

Read Online

ACCESS | Metrics & More | Article Recommendations

ABSTRACT: Herein, we introduce a novel composite hydrogel scaffold designed for addressing infectious jaw defects, a significant challenge in clinical settings caused by the inherent limited self-regenerative capacity of bone tissues. The scaffold was engineered from a blend of carboxymethyl chitosan (CMCS)/sodium alginate (SA) hydrogel (CSH), β-cyclodextrin/chlorhexidine clathrate (β-CD-CHX), and strontium-nanohydroxyapatite nanoparticles (Sr-nHA). The β-CD-CHX and Sr-nHA components were synthesized using a saturated aqueous solution and a coprecipitation method, respectively. Subsequently, these elements were encapsulated within the CSH matrix. Comprehensive characterization of the CMCS/SA/β-CD-CHX/Sr-nHA composite hydrogel scaffold via scanning electron microscopy, X-ray photoelectron spectroscopy, and Fourier-transform infrared spectroscopy validated the successful synthesis. The swelling and *in vitro* degradation behaviors proved that the composite hydrogel had good physical properties, while *in vitro* evaluations demonstrated favorable biocompatibility and osteoinductive properties. Additionally, antibacterial assessments revealed its effectiveness against common pathogens, *Staphylococcus aureus* and *Escherichia coli*. Overall, our results indicate that the CMCS/SA/β-CD-CHX/Sr-nHA composite hydrogel scaffolds exhibit significant potential for effectively treating infection-prone jaw defects.

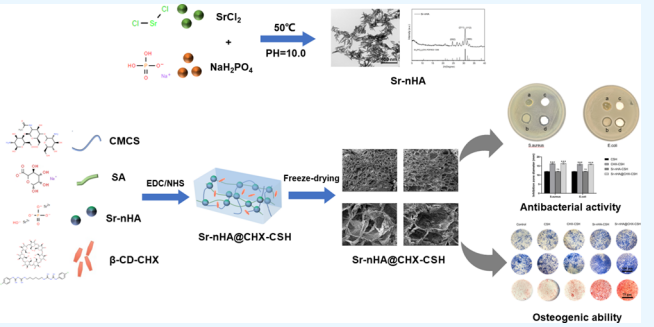

1. INTRODUCTION

The rising incidence of jaw defects due to factors such as inflammation, trauma, tumors, and congenital malformations poses a significant challenge in clinical care, particularly regarding the safe and effective repair and reconstruction of these defects.[1,2] Maxillofacial defects profoundly affect not only the normal function and facial aesthetics of patients but also have adverse effects on their physical and mental health.[3,4] Bone defects in the oral and maxillofacial areas are often situated in anatomically complex sites that are prone to bacterial infection, producing a high risk of postoperative bacterial infection following the reconstruction of jaw defects.[5,6] *Staphylococcus aureus* is the primary pathogen responsible for these infections.[7] Severe bacterial infections can complicate treating jaw defects, potentially increasing wound size and the likelihood of developing serious osteomyelitis.[8,9] Consequently, managing local infections and fostering bone healing are critical aspects of bone repair.[10] The development of a biomaterial that possesses both antimicrobial and osteogenic properties is therefore of significant clinical importance for treating jaw defects susceptible to infection.[11]

Hydrogels are highly hydrophilic polymers that form an interconnected three-dimensional (3D) porous network through cross-linking[12] and have found extensive application in biomedical fields because of their exceptional biocompatibility, hydrophilicity, and drug-delivery capabilities.[13,14] Recent advancements in hydrogel technology have shown promising results in enhancing cellular bioactivity and achieving effective antimicrobial outcomes, thereby opening new therapeutic possibilities for treating jaw defects.[15] Chitosan-based hydrogels, in particular, have garnered significant attention in biomedical research, especially for drug delivery applications because of their excellent biocompatibility, cell adhesion properties, biodegradability, antimicrobial efficacy, and stability.[16−18] Carboxymethyl

Received: February 7, 2024
Revised: April 4, 2024
Accepted: April 30, 2024
Published: May 12, 2024

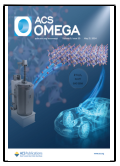

chitosan (CMCS) is a derivative of chitosan, obtained through carboxymethylation. CMCS surpasses chitosan in several aspects, including water solubility, moisture retention, antioxidant, antibacterial, and antifungal properties, and is therefore a highly promising material for drug delivery and tissue engineering.[19−21] Sodium alginate (SA), a naturally occurring polysaccharide sourced from brown algae, has also gained significant biomedical interest because of its outstanding antioxidant properties, biodegradability, biocompatibility, and cost-effectiveness, making it a valuable component in various biomedical applications.[22,23]

Chlorhexidine (CHX), a cationic bisguanidine, is frequently utilized in dentistry owing to its outstanding broad-spectrum antimicrobial activity.[24] β-cyclodextrin (β-CD) has been employed to encapsulate CHX within inclusion complexes using the saturated ethanol solution technique. These complexes have demonstrated potent sustained release and antibacterial properties. The deployment of β-CD is crucial in modulating the release of CHX, providing a controlled delivery mechanism that enhances its effectiveness in clinical applications.[25−27]

To overcome the limitations of conventional hydrogels, such as poor mechanical properties and insufficient antimicrobial capacity, researchers have been developing hydrogels endowed with antimicrobial and osteoinductive features.[7,28,29] These hydrogels incorporate ceramic materials such as nanohydroxyapatite (nHA) and antimicrobial agents. nHA shares structural and biochemical similarities with the mineral composition of animal and human bone tissues and is considered an ideal material for bone defect healing due to its exceptional biocompatibility, osteoconductivity, osteoinductivity, and bioactivity.[30−32] Recent studies showed that incorporating metal ions into nHA can significantly improve the mechanical, biological, and antimicrobial characteristics. Various metal ions, such as Y^{3+}, Zn^{2+}, Mn^{2+}, Mg^{2+}, Sr^{2+}, Ti^{4+}, or Ag^{2+}, have been doped into nHA to enhance the physicochemical attributes;[33−36] the selected dopant must improve the physicochemical properties of nHA without compromising its biological efficacy.[37] Among these, Sr^{2+}, a trace element in human bone tissue, is known for its osteoinductive properties, biocompatibility, and relevance in treating osteoporosis.[38,39] The biological prowess of Sr^{2+} has increased the focus on developing strontium-nanohydroxyapatite (Sr-nHA) in recent years. Studies have validated that Sr-nHA not only promotes cell adhesion and growth but also stimulates osteoblast activity and inhibits osteoclasts *in vitro*.[37,39] Ding et al. highlighted that varying levels of strontium doping in nHA produced different effects on bone regeneration, with Sr-nHA having a 100% Sr/Ca + Sr molar ratio and exceptional osteogenic properties.[40]

While previous research has established the promising osteogenic properties of Sr-nHA,[40] significant evidence has demonstrated the robust antibacterial characteristics of β-CD-CHX.[25] However, few systematic studies have explored the encapsulation of β-CD-CHX with Sr-nHA in composite hydrogel scaffolds. Thus, this study focused on the design and development of Sr-nHA nanoparticles and the incorporation of β-CD-CHX into CMCS/SA hydrogels. The primary objective was to comprehensively investigate the properties, *in vitro* biocompatibility, bone regeneration potential, and antimicrobial efficacy of these novel composite hydrogel scaffolds. Our aim was to create a filler material tailored for treating jaw defects that offers the dual benefits of antimicrobial and osteogenic properties that are crucial for repairing jaw defects in scenarios with a risk of infection.

2. EXPERIMENTAL SECTION

2.1. Materials. β-CD was sourced from Shanghai Boao Biotechnology, and CHX was procured from Sigma-Aldrich. CMCS, SA, and NaH_2PO_4 were acquired from Dalian Meilun Biotechnology Co., Ltd. Cross-linking agents 1-ethyl-(3-(dimethylamino)propyl)carbodiimide hydrochloride (EDC) and *N*-hydroxysuccinimide (NHS) were supplied by Shanghai Aladdin Biochemical Technology Co., Ltd. $SrCl_2$ and ammonium hydroxide ($NH_3{\cdot}H_2O$) were obtained from Shanghai Macklin Biochemical Co., Ltd.

2.2. Preparation and Characterization of Sr-nHA. Sr-nHA was synthesized using the coprecipitation technique.[40] A solution of NaH_2PO_4 was gradually added to a vigorously stirred $SrCl_2$ solution, maintaining a Sr/P molar ratio of 5:3, and $NH_3{\cdot}H_2O$ was used to adjust the pH of the reaction mixture to 10.0. The reaction proceeded at 50 °C for 1 h, followed by continuous stirring for an additional 2 h, and then left to age for 24 h at ambient temperature. The resultant precipitate was then filtered and thoroughly washed three times with anhydrous ethanol, followed by three washes with distilled water. Subsequently, the material was freeze-dried, yielding Sr-nHA with a $Sr^{2+}/(Ca^{2+} + Sr^{2+})$ molar ratio of 100%. Sr-nHA was characterized with transmission electron microscopy (TEM) (Jeol/JEM 2100, USA), and qualitative analysis was conducted via Fourier-transform infrared spectroscopy (FTIR; NEXUS-470, Thermo Nicolet, USA). The elemental composition of Sr-nHA was determined using X-ray photoelectron spectroscopy (XPS; ESCALAB250XI, USA). The crystal structure of Sr-nHA was measured via X-ray diffraction (XRD; D8 Advance, Germany).

2.3. Preparation and Characterization of Composite Hydrogel Scaffolds. β-CD-CHX was synthesized using the saturated aqueous solution method. β-CD was first dissolved in double-distilled water to create a saturated solution, while CHX was dissolved in ethanol to achieve a 1:1 molecular ratio with β-CD. The CHX solution was then incrementally added to the stirred β-CD solution. The reaction proceeded at 50 °C for 1 h. Subsequently, the mixture was cooled, filtered, and ground to yield CHX/β-CD powder through evaporation and further grinding. EDC and NHS were used as the cross-linking agents to fabricate the hydrogel. SA was grafted onto CMCS to form CMCS/SA hydrogels (CSH), as previously described.[41] For this, 0.15 g of CMCS was dissolved in 5 mL of a 0.9% NaCl solution at room temperature, and 0.15 g of SA was dissolved in 5 mL of deionized water. After thorough stirring, the CMCS/SA mixture was obtained. Then, 112.5 mg each of EDC and NHS were added to 10 mL of the CMCS/SA solution and stirred for 1 h to activate the carboxyl group of SA. The mixture was then left to react for 12 h to yield the CSH hydrogel. To integrate β-CD-CHX and Sr-nHA, they were added to the CMCS/SA solution and stirred for 1 h, ensuring a uniform dispersion. The final concentrations were set at 0.1% (w/v) for β-CD-CHX and 6% (w/v) for Sr-nHA. Following this, hydrogels such as CSH, CHX-CSH (containing β-CD-CHX), Sr-nHA-CSH (containing Sr-nHA), and Sr-nHA@CHX-CSH (containing both β-CD-CHX and Sr-nHA) were prepared. Composite hydrogel scaffolds were characterized using scanning electron microscopy (SEM). Qualitative analysis of the hydrogels was conducted using FTIR, and the elemental compositions were analyzed via XPS.

https://doi.org/10.1021/acsomega.4c01237
ACS Omega 2024, 9, 22230−22239

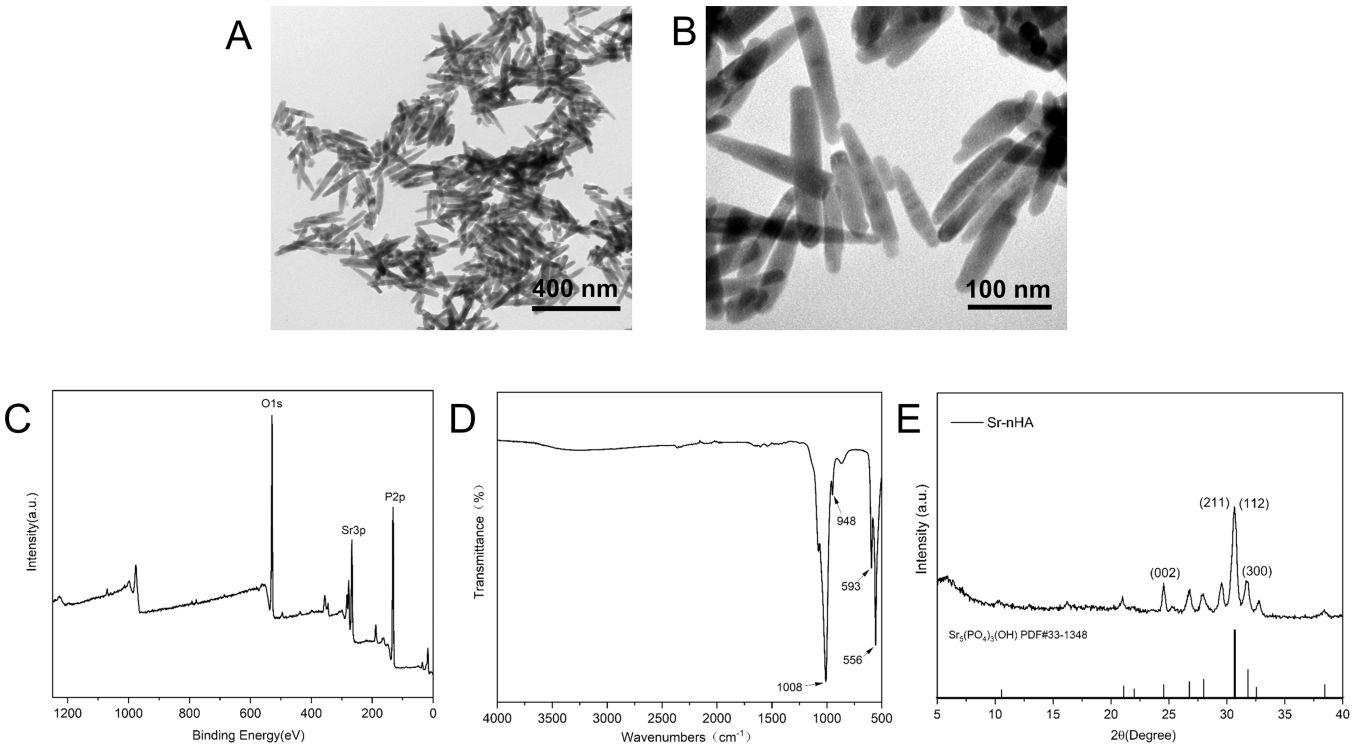

Figure 1. TEM image of Sr-nHA (A,B), XPS spectra (C), FTIR spectra (D), and XRD spectra (E) of Sr-nHA.

2.4. Physical Properties. *2.4.1. Swelling Study.* The lyophilized hydrogel sample was weighed (W_0) and soaked in 5 mL of PBS for 48 h to achieve swelling equilibrium, and then the hydrogel surface solution was blotted with filter paper before weighing the expanded hydrogel (W_1). The swelling ratio of the hydrogel was calculated as follows:

$$\text{Swelling ratio} = (W_1 - W_0)/W_0 \times 100\%$$

2.4.2. Degradation Behavior. The masses (W_0) of the four lyophilized hydrogel groups were weighed. Subsequently, the hydrogels were immersed in 5 mL of PBS at 37 °C. The hydrogels were then removed from PBS at different time points, lyophilized, and weighed (W_t). The degree of in vitro degradation was calculated using the following equation:

$$\text{Remaining}\ (\%) = W_t/W_0 \times 100\%$$

2.5. Cell Proliferation Assessment. The experimental setup included five groups: control, CSH, CHX-CSH, Sr-nHA-CSH, and Sr-nHA@CHX-CSH groups. After fabrication, the hydrogels were sterilized under UV light for 2 h and then soaked in a cell culture medium that contained 1% penicillin/streptomycin and 10% fetal bovine serum. Extracts from these hydrogels were collected after 24 h at 37 °C and stored at 4 °C. The effect of these hydrogel scaffolds on cell proliferation was evaluated using MC3T3-E1 cells. These cells were seeded in 96-well plates at 5×10^3 cells per well and incubated at 37 °C with 5% CO_2. Each group had five replicated samples prepared. On days 1, 3, and 5 after seeding, 10 μL of CCK-8 solution was added to each well and incubated for 1 h. The absorbance was measured at 450 nm using an enzyme marker to assess cell proliferation. Additionally, cell proliferation was visualized using AM/PI staining after 1, 3, and 5 days of incubation. Stained cells were observed under fluorescence microscopy to analyze cell proliferation patterns.

2.6. Cell Osteogenic Differentiation. To prepare the osteogenic induction medium for each group, 10 mmol/L sodium β-glycerophosphate, 50 μg/mL ascorbic acid, and 0.1 μmol/L dexamethasone were added to the extracts. MC3T3-E1 (ATCC, CRL-2594) cells were then cultured in 12-well plates. Once the cell density had reached 80%, the medium was replaced with the osteogenic induction medium, which was subsequently changed every 2 days. ALP staining was performed using ALP kits from the Nanjing Jianjian Bioengineering Institute and from the Dalian Meilunbio Bioengineering Institute after 7 and 14 days of culture. For mineralization analysis, cells were fixed in 4% paraformaldehyde for 30 min on day 21. Each well was then treated with a 2% alizarin red solution (provided by Dalian Meilunbio Bioengineering Institute) and incubated for 45 min. Samples were observed under a microscope and photographed. To dissolve the calcium nodules, each well was treated with 100 nmol/L cetylpyridinium chloride at room temperature for 30 min. Optical density values were measured using a microplate reader at 562 nm.

2.7. *In Vitro* Antibacterial Activity. The antimicrobial properties of the hydrogels were assessed by measuring the diameters of the inhibition zones surrounding cultures of *S. aureus* and *E. coli*. Hydrogels were fashioned into cylinders with a 12-mm diameter and a 5-mm height and then sterilized under UV light for 2 h before use. A 200-μL volume each of *S. aureus* (ATCC 6538) and *E. coli* (ATCC 8739) cultures was uniformly spread on sterile Luria−Bertani (LB) agar plates and incubated at 37 °C for 1 h. Subsequently, hydrogels from each group were placed on LB agar plates containing bacteria and incubated at 37 °C for 24 h. Plates were photographed after incubation, and the dimensions of the zones of inhibition were measured.

2.8. Statistical Analysis. Each experiment was conducted in triplicate, ensuring independent replication for each set.

https://doi.org/10.1021/acsomega.4c01237
ACS Omega 2024, 9, 22230−22239

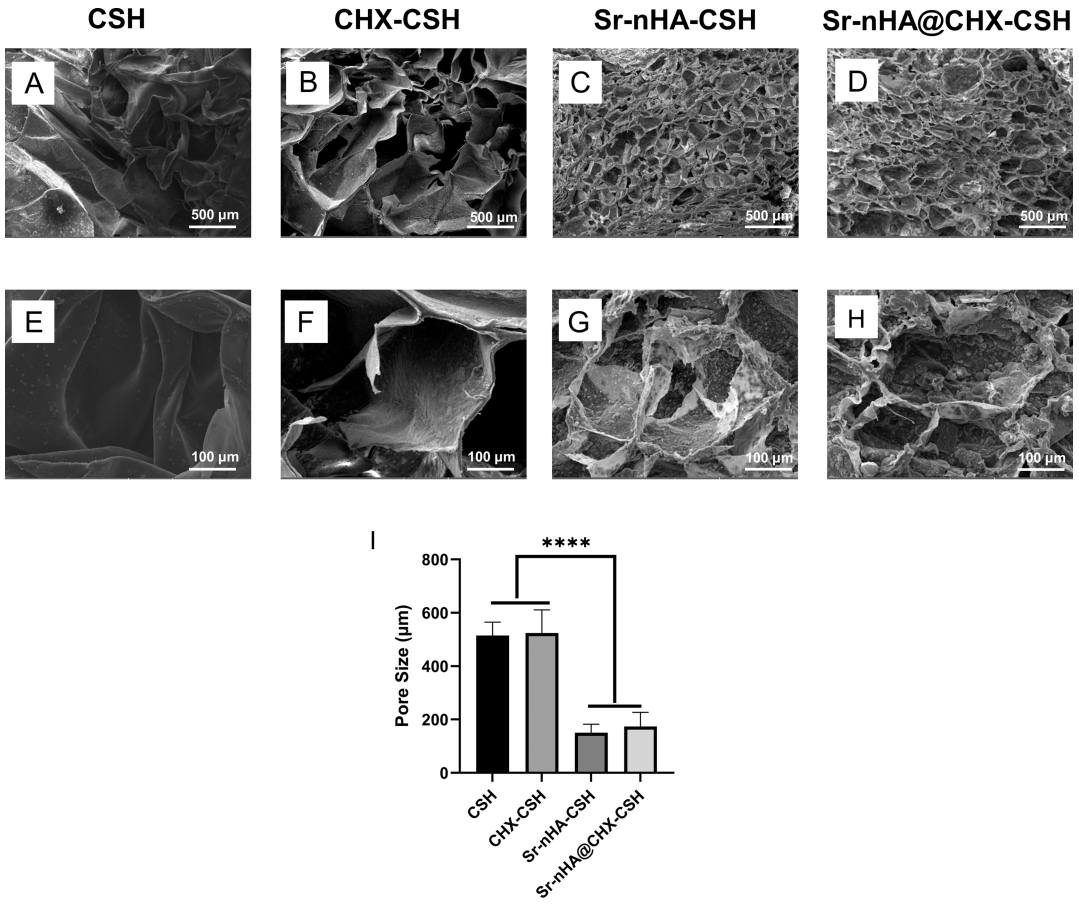

Figure 2. SEM images of CSH, CHX-CSH, Sr-nHA-CSH, and Sr-nHA@CHX-CSH (A–D: 100×, E–H: 500×). (I) Pore size of hydrogels.

Data analysis was performed using GraphPad Prism 9 software, with results presented as the mean ± standard deviation. For group comparisons, one-way analysis of variance was employed. The significance levels are indicated as follows: $*P < 0.05$, $**P < 0.01$, and $***P < 0.001$.

3. RESULTS AND DISCUSSION

3.1. Characterization of Sr-nHA. Representative TEM images of Sr-nHA nanoparticles showed a regular rod-like morphology that was consistent with that seen in prior research (Figure 1A,B);[42] additionally, slightly darker areas were present, indicative of the stacking of the Sr-nHA nanoparticles. The XPS spectra (Figure 1C) validated the presence of elements O, P, and Sr in Sr-nHA with binding energies at approximately 529, 132, and 267 eV, respectively. The FTIR spectrum of Sr-nHA (Figure 1D) exhibited the characteristic absorption peaks of PO_4^{3-} at 1008, 948, 593, and 556 cm^{-1}. Furthermore, the presence of hydroxyl groups was corroborated by the weaker, broader bands observed in the 3600–3000 cm^{-1} range. The XRD pattern of Sr-nHA was consistent with that of the standard card JCPDS #33-1348 ($Sr_5(PO_4)_3(OH)$) (Figure 1E). The diffraction peaks at 24.45°, 30.5°, and 31.72° are considered to belong to the (002), (211), and (300) crystal planes, which are typical of the characteristic diffraction peaks of Sr-nHA and are consistent with results from previous studies.[40,43] Collectively, the TEM, XPS, FTIR, and XRD analyses substantiated the successful synthesis of Sr-nHA nanoparticles.

3.2. Characterization of Composite Hydrogel Scaffolds. The microstructural morphology of four varieties of lyophilized composite hydrogel scaffolds is shown in SEM images in Figure 2. Each group of scaffolds exhibited a 3D porous structure, with pores caused by the formation of ice crystals during the freeze-drying process.[44] This 3D porous structure is advantageous for promoting cell proliferation and nutrient transportation.[45] The CSH hydrogel, in particular, exhibited comparatively smooth pore walls (Figure 2A,E). The introduction of β-CD-CHX into CSH did not alter the 3D porous architecture of the hydrogel. However, under high magnification, the pore walls of the CHX-CSH hydrogels appeared marginally rougher than those of the CSH group, with occasional protruding particles noticeable on the surface (Figure 2F). The incorporation of Sr-nHA further roughened the surface texture of both Sr-nHA-CSH and Sr-nHA@CHX-CSH scaffolds (Figure 2C,D,G,H), with a more pronounced presence of protruding particles. This is probably due to the dispersion of nanoparticles on the scaffold surfaces, which causes a degree of agglomeration.[40] Surface roughness has been reported to be critical for cell adhesion to hydrogels, and an increase in surface roughness causes a subsequent increase in the surface area of the hydrogel, which provides more adhesion sites for cells and favors cell proliferation and new bone formation.[46] The average pore sizes of CSH, CHX-CSH, Sr-nHA-CSH, and Sr-nHA@CHX-CSH were 515.16 ± 49.92, 524.11 ± 86.64, 150.30 ± 32.07, and 173.99 ± 52.72 um, respectively. The pore sizes of Sr-nHA-CSH and Sr-nHA@CHX-CSH were significantly smaller than those of CSH and CHX-CSH, which may be attributed to the increase in the degree of cross-linking of the hydrogel upon the addition of Sr-nHA, producing a denser lattice.[47] Suitable pore sizes facilitate

https://doi.org/10.1021/acsomega.4c01237
ACS Omega 2024, 9, 22230–22239

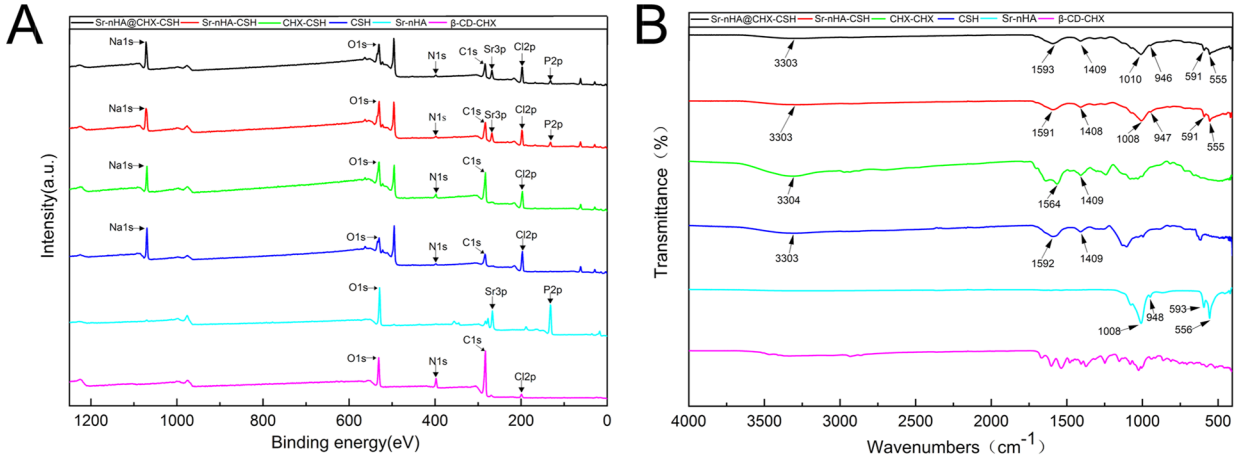

Figure 3. (A) XPS spectra and (B) FTIR spectra of β-CD-CHX, Sr-nHA, CSH, CHX-CSH, Sr-nHA-CSH, and Sr-nHA@CHX-CSH.

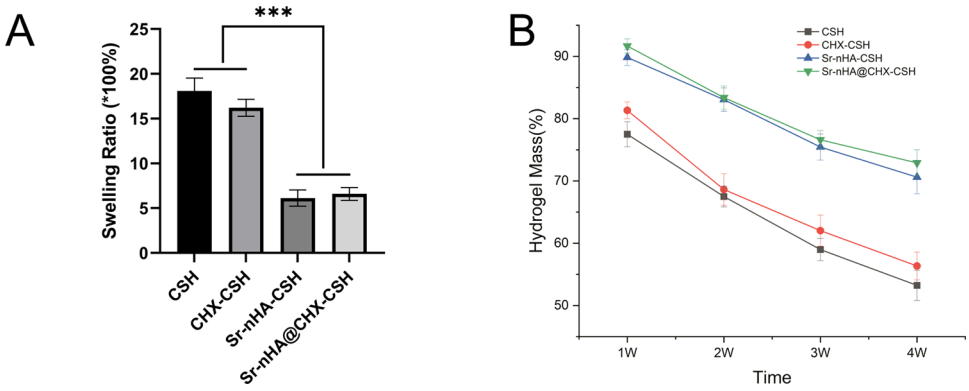

Figure 4. Equilibrium swelling studies (A) and the degradation test (B) of CSH, CHX-CSH, Sr-nHA-CSH, and Sr-nHA@CHX-CSH.

cellular material exchange and metabolic waste discharge.[48] Sr-nHA@CHX-CSH had a pore size similar to that of human cancellous bone (pore size: 100−200 μm), which is crucial for bone repair.[49] A 100−300-μm pore size of the scaffold has been proven to be the most suitable for the growth of osteoblasts.[50] Thus, we constructed Sr-nHA@CHX-CSH hydrogels with a 3D porous structure, suitable pore size, and rough surface, which are expected to provide a favorable environment for bone repair.

The XPS analysis indicated that Sr-nHA@CHX-CSH contains C, N, O, P, Na, Cl, and Sr (Figure 3A). This composition aligns with the total elemental constitution of Sr-nHA, β-CD-CHX, and CSH. Notably, the XPS spectrum of Sr-nHA-CSH displayed P 2p and Sr 3p peaks that were absent in that of CSH. The O/C ratios for Sr-nHA@CHX-CSH (1.17) and Sr-nHA-CSH (1.10) exceeded those of CSH (0.47), implying that the incorporation of β-CD-CHX and Sr-nHA contributes additional O atoms and modifies the chemical structure of the hydrogel surface.[11] These XPS findings confirm the successful creation of the composite hydrogels.

The FTIR spectrum of CSH (Figure 3B) exhibited broad peaks at 3303 cm^{-1}, indicative of the −OH and $-NH_2$ stretching vibration absorptions. Additionally, peaks at 1592 and 1409 cm^{-1} were observed, corresponding to the asymmetric and symmetric stretching vibrations of the carboxyl group, respectively. With the incorporation of Sr-nHA, the Sr-nHA-CSH sample revealed characteristic $-PO_4$ peaks at 1008, 947, 591, and 555 cm^{-1}. The FTIR spectrum of Sr-nHA@CHX-CSH demonstrates peaks similar to those of Sr-nHA-CSH, suggesting that the structural integrity of the composite hydrogel remained largely unchanged after the addition of β-CD-CHX. Notably, the Sr-nHA@CHX-CSH spectrum encompassed all characteristic peaks of its constituents (β-CD-CHX, Sr-nHA, and CSH). This comprehensive spectral representation is indicative of the successful synthesis of the composite hydrogel through the physical comingling of its components. Furthermore, the addition of β-CD-CHX and Sr-nHA to CSH did not appear to alter the chemical structure and composition of the original CSH matrix, which is consistent with the results obtained from XPS analysis.

3.3. Physical Properties. *3.3.1. Swelling Study.* As shown in Figure 4A, all 4 groups of hydrogels showed favorable swelling characteristics, with average swelling rates of 1809.83% ± 144.06%, 1621.25% ± 95.09%, 612.01% ± 82.05%, and 658.43% ± 52.98% for CSH, CHX-CSH, Sr-nHA-CSH, and Sr-nHA@CHX-CSH, respectively. The swelling of the hydrogels was significantly reduced by the incorporation of Sr-nHA, which was attributed to the hydrophobicity of Sr-nHA and the filling of the pores of the hydrogels with Sr-nHA after incorporation, as this reduced the water storage space of the hydrogel.[51]

3.3.2. Degradation Behavior. The remaining amounts of CSH, CHX-CSH, Sr-nHA-CSH, and Sr-nHA@CHX-CSH amounted to 53.23% ± 2.42%, 56.34 ± 2.23%, 70.61 ± 2.71%, and 72.89 ± 2.11% by the fourth week (Figure 4B).

https://doi.org/10.1021/acsomega.4c01237
ACS Omega 2024, 9, 22230−22239

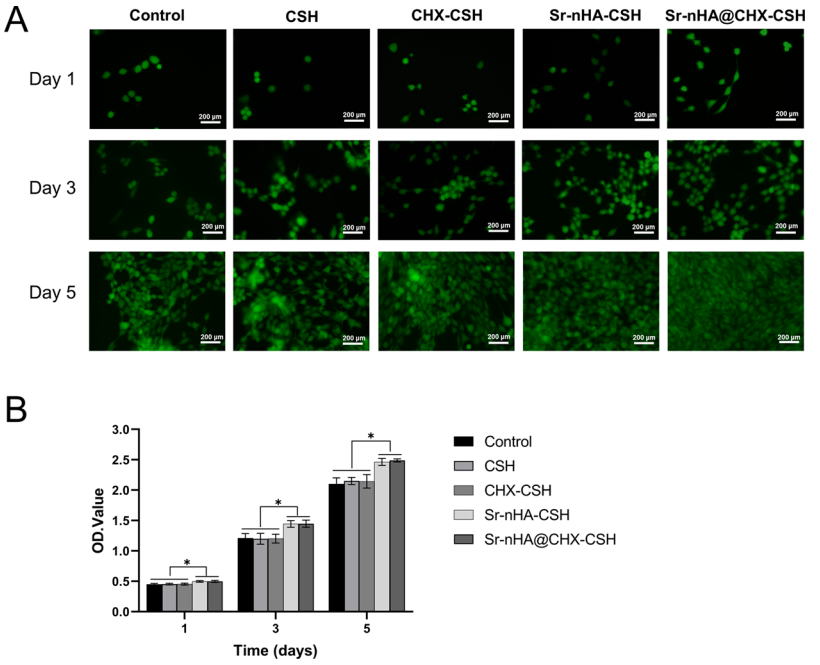

Figure 5. AM/PI staining images (A) and cell proliferation evaluation of Control, CSH, CHX-CSH, Sr-nHA-CSH, and Sr-nHA@CHX-CSH groups for 1, 3, and 5 days (B).

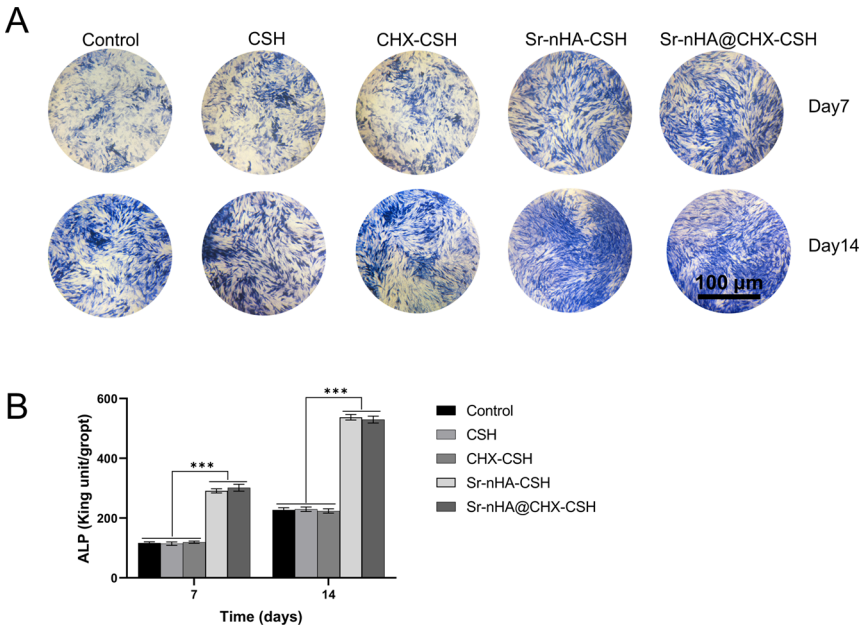

Figure 6. ALP staining images (A) and quantitative analysis of ALP activity (B) after 7 and 14 days of culture.

The degradation rate of hydrogel was reduced by the addition of Sr-nHA compared with that of CSH and CHX-CSH, which was attributed to the introduction of a large number of divalent cations and the enhancement of the cross-linking density of the hydrogel by the addition of Sr-nHA.[52] Hydrogel scaffolds require a certain amount of degradation to consistently release nanoparticles for their antimicrobial and osteogenic capabilities.[53]

3.4. Cell Proliferation. MC3T3-E1 cells were incubated with hydrogels for 1, 3, and 5 days, and the cells were then stained with AM/PI and observed for cell proliferation using a fluorescence microscope. Over time, the number of cells noticeably increased across all five groups. Both the Sr-nHA-CSH and Sr-nHA@CHX-CSH groups exhibited a significantly higher count of MC3T3-E1 cells than that in the control, CSH, and CHX-CSH groups (Figure 5A). The OD values between the CSH and CHX-CSH groups did not significantly differ, nor did the values between the Sr-nHA-CSH and Sr-nHA@CHX-CSH groups (Figure 5B). This indicates that the addition of β-CD-CHX did not affect cell viability. However, the cell counts in both the Sr-nHA-CSH and Sr-nHA@CHX-CSH groups were significantly higher than those in the control, CSH, and CHX-CSH groups ($P < 0.05$). The higher cell proliferation rates in the Sr-nHA-CSH and Sr-nHA@CHX-CSH groups could be attributed to the improved roughness of the hydrogels after loading with Sr-nHA, which provided more adhesion sites

https://doi.org/10.1021/acsomega.4c01237
ACS Omega 2024, 9, 22230−22239

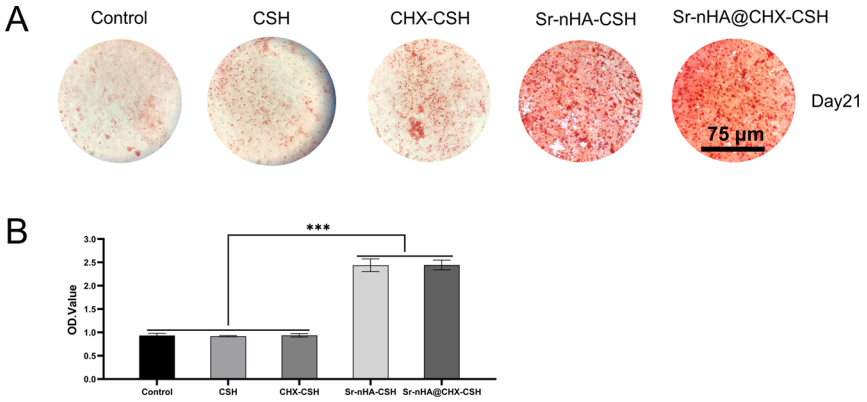

Figure 7. ARS staining images (A) and quantitative analysis of cell mineralization (B) after 7 and 14 days of culture.

for the cells and thus effectively promoted cell proliferation. Furthermore, Sr^{2+} from Sr-nHA has been reported to promote the proliferation of MC3T3-E1 cells.[54] Thus, the Sr-nHA@CHX-CSH hydrogel demonstrated excellent cytocompatibility, making this a promising material for bone implants, particularly for treating bone defects.

3.5. Cell Osteogenic Differentiation Experiment. After 7 and 14 days of osteogenic induction, both the Sr-nHA-CSH and Sr-nHA@CHX-CSH groups exhibited noticeably more pronounced ALP staining than that in the control, CSH, and CHX-CSH groups (Figure 6A). This enhanced ALP staining suggests an accelerated differentiation of MC3T3-E1 cells into osteoblasts in these groups, with a larger number of cells undergoing differentiation. The quantitative ALP analysis (Figure 6B) indicates significantly higher ALP activity in the Sr-nHA-CSH and Sr-nHA@CHX-CSH groups than that in the control, CSH, and CHX-CSH groups ($P < 0.001$). Interestingly, the quantitative analysis of ALP staining in the control, CSH, and CHX-CSH groups revealed no statistical difference between these, indicating that the incorporation of β-CD-CHX into the hydrogels did not significantly affect their ability to stimulate osteogenic differentiation. The mineralization of cells after 21 days of osteogenic induction (Figure 7A,B) is a critical phase in late osteogenesis. Both the Sr-nHA-CSH and Sr-nHA@CHX-CSH groups showed enhanced deposition of calcium and higher levels of mineralization compared with those in the control, CSH, or CHX-CSH groups because of the excellent osteoinductivity of the Sr^{2+} element and nHA.[48,54,55] This was consistently evident in both the calcium nodule staining and the quantitative analysis of it. In addition, the porous structure and rough surface of hydrogels provide a large specific surface area that is conducive to increasing cell activity and promoting tissue infiltration, which consequently promotes osteogenic differentiation of cells.[48]

Thus, the efficacy of Sr-nHA@CHX-CSH in promoting osteogenic differentiation and mineralization was effectively verified by using *in vitro* cellular osteogenic induction experiments and shown to display a good application prospect in treating bone defects.

3.6. Antibacterial Experiment. The presence of inhibitory rings around CHX-CSH and Sr-nHA@CHX-CSH is shown in Figure 8. Notably, the inhibitory rings of CHX-CSH and Sr-nHA@CHX-CSH did not significantly differ, whereas these were nearly imperceptible for CSH and Sr-nHA-CSH; these results were confirmed by histogram analysis (Figure 8B), where CHX-CSH and Sr-nHA@CHX-CSH produced

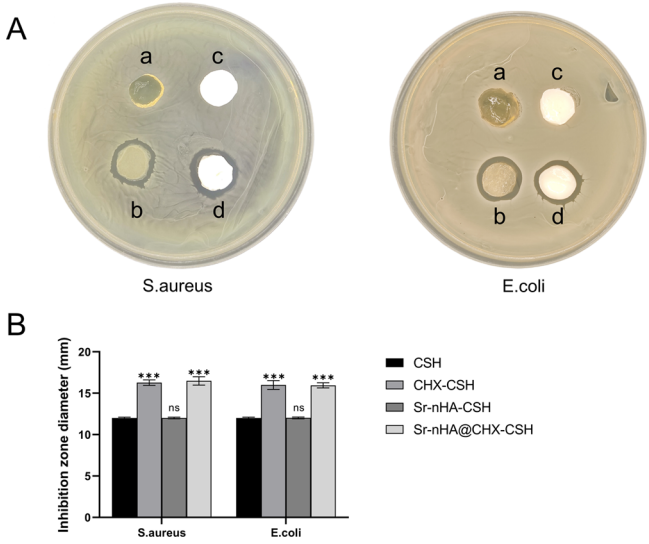

Figure 8. Antibacterial test results (A) and the diameter of the inhibition zone (B) for *S. aureus* and *E. coli* of CSH (a), CHX-CSH (b), Sr-nHA-CSH (c), and Sr-nHA@CHX-CSH (d).

significantly larger zones of inhibition compared with those of CSH and Sr-nHA-CSH ($P < 0.001$). Thus, incorporation of β-CD-CHX into the hydrogels notably enhanced their antimicrobial capabilities against *S. aureus* and *E. coli*.[25] However, the addition of Sr-nHA did not markedly improve the antimicrobial properties of the composite hydrogels. Therefore, the results from Figure 7 indicate that Sr-nHA@CHX-CSH has effective antimicrobial properties against *S. aureus* and *E. coli*. The healing process of jaw defects has a high risk of infection because of the specifics of this anatomical site.[5,6] Sr-nHA@CHX-CSH can provide a favorable anti-infective effect and has a good prospect for oral clinical application.

4. CONCLUSIONS

This study successfully synthesized composite hydrogel scaffolds exhibiting commendable osteogenic and antibacterial properties. SEM analysis of the surface morphology of these scaffolds revealed a porous structure with a rough surface texture on the pore walls, which is conducive to cell adhesion. The successful incorporation of β-CD-CHX and Sr-nHA into the composite hydrogel scaffolds was verified via FTIR and XPS analyses. The favorable hydrophilicity and biodegradability of the composite hydrogel were revealed by the analysis

https://doi.org/10.1021/acsomega.4c01237
ACS Omega 2024, 9, 22230−22239

of the swelling and *in vitro* degradation behavior. Notably, the hydrogel scaffold demonstrated impressive biocompatibility and antimicrobial efficacy. Furthermore, the hydrogel exhibited a marked capacity to induce osteogenic differentiation and mineralization in osteoblasts. Thus, these hydrogel scaffolds hold significant potential for treating jaw defects, particularly in cases where an elevated risk of infection is present.

AUTHOR INFORMATION

Corresponding Authors

Jian Sun − *Department of Oral and Maxillofacial Surgery, The Affiliated Hospital of Qingdao University, Qingdao 266003, China; School of Stomatology, Qingdao University, Qingdao 266003, China; Dental Digital Medicine and 3D Printing Engineering Laboratory of Qingdao, Qingdao 266003, China; The Climbing Peak Discipline Project of Qingdao, Qingdao 266003, China*; Email: sunjianqdfy@qdu.edu.cn

Liqiang Chen − *Department of Oral and Maxillofacial Surgery, The Affiliated Hospital of Qingdao University, Qingdao 266003, China; School of Stomatology, Qingdao University, Qingdao 266003, China; Dental Digital Medicine and 3D Printing Engineering Laboratory of Qingdao, Qingdao 266003, China; The Climbing Peak Discipline Project of Qingdao, Qingdao 266003, China*; Email: clqiang1010@163.com

Authors

Zijian Liu − *Department of Oral and Maxillofacial Surgery, The Affiliated Hospital of Qingdao University, Qingdao 266003, China; School of Stomatology, Qingdao University, Qingdao 266003, China*; orcid.org/0009-0008-5941-1935

Shangbo Li − *Department of Oral and Maxillofacial Surgery, The Affiliated Hospital of Qingdao University, Qingdao 266003, China; School of Stomatology, Qingdao University, Qingdao 266003, China*

Zexian Xu − *Department of Oral and Maxillofacial Surgery, The Affiliated Hospital of Qingdao University, Qingdao 266003, China; School of Stomatology, Qingdao University, Qingdao 266003, China*

Li Li − *Department of Oral and Maxillofacial Surgery, The Affiliated Hospital of Qingdao University, Qingdao 266003, China; School of Stomatology, Qingdao University, Qingdao 266003, China*

Yanshan Liu − *Department of Oral and Maxillofacial Surgery, The Affiliated Hospital of Qingdao University, Qingdao 266003, China; School of Stomatology, Qingdao University, Qingdao 266003, China; Dental Digital Medicine and 3D Printing Engineering Laboratory of Qingdao, Qingdao 266003, China*

Xiaohan Gao − *Department of Oral and Maxillofacial Surgery, The Affiliated Hospital of Qingdao University, Qingdao 266003, China; School of Stomatology, Qingdao University, Qingdao 266003, China*

Yaru Diao − *Department of Oral and Maxillofacial Surgery, The Affiliated Hospital of Qingdao University, Qingdao 266003, China; School of Stomatology, Qingdao University, Qingdao 266003, China*

Complete contact information is available at: https://pubs.acs.org/10.1021/acsomega.4c01237

Author Contributions

All the authors have significantly contributed to the reported work. The final version of the paper is approved by all the authors.

Notes

The authors declare no competing financial interest.

ACKNOWLEDGMENTS

The author(s) declare that financial support was received for the research, authorship, and/or publication of this article. This research was funded by the Qingdao Medical and Health Research Plan Project Funding (grant number: 2021-WJZD193), the Funding for the "Clinical Medicine + X Project" of Qingdao University Hospital (grant number: QDFY+X202101041, QDFY+X2023207), the Shandong Provincial Medical and Health Science and Technology Development Plan Project (grant number: 202208020979, 202308020875), the Qingdao Medical and Health Key Discipline Construction Project Funding, the Qingdao Stomatology Climbing Peak Discipline Project (grant number: 2022-11-29-07), and the Qingdao City South District Science and Technology Plan Project (grant number: 2023-2-005-YY).

REFERENCES

(1) Deng, N.; Sun, J.; Li, Y.; Chen, L.; Chen, C.; Wu, Y.; Wang, Z.; Li, L. Experimental study of rhBMP-2 chitosan nano-sustained release carrier-loaded PLGA/nHA scaffolds to construct mandibular tissue-engineered bone. *Archives of Oral Biology* **2019**, *102*, 16.

(2) Mehrabani, D.; Khodakaram-Tafti, A.; Shaterzadeh-Yazdi, H.; Zamiri, B.; Omidi, M. Comparison of the regenerative effect of adipose-derived stem cells, fibrin glue scaffold, and autologous bone graft in experimental mandibular defect in rabbit. *Dental traumatology: official publication of International Association for Dental Traumatology* **2018**, *34* (6), 413.

(3) Xu, Z.; Li, Y.; Xu, D.; Li, L.; Xu, Y.; Chen, L.; Liu, Y.; Sun, J. Improvement of mechanical and antibacterial properties of porous nHA scaffolds by fluorinated graphene oxide. *RSC Adv.* **2022**, *12* (39), 25405.

(4) Zhang, C.; Zhou, Z.; Liu, N.; Chen, J.; Wu, J.; Zhang, Y.; Lin, K.; Zhang, S. Osteogenic differentiation of 3D-printed porous tantalum with nano-topographic modification for repairing craniofacial bone defects. *Front. Bioeng. Biotechnol.* **2023**, *11*, No. 1258030, DOI: 10.3389/fbioe.2023.1258030.

(5) Ghosh, S.; Sinha, M.; Samanta, R.; Sadhasivam, S.; Bhattacharyya, A.; Nandy, A.; Saini, S.; Tandon, N.; Singh, H.; Gupta, S.; Chauhan, A.; Aavula, K. K.; Varghese, S. S.; Shi, P.; Ghosh, S.; Garg, M. K.; Saha, T.; Padhye, A.; Ghosh, S.; Jang, H. L.; Sengupta, S. A potent antibiotic-loaded bone-cement implant against staphylococcal bone infections. *Nature Biomedical Engineering* **2022**, *6* (10), 1180.

(6) Feng, P.; He, R.; Gu, Y.; Yang, F.; Pan, H.; Shuai, C. Construction of antibacterial bone implants and their application in bone regeneration. *Mater. Horiz.* **2024**, *11*, 590 DOI: 10.1039/D3MH01298K.

(7) Xu, L.; Ye, Q.; Xie, J.; Yang, J.; Jiang, W.; Yuan, H.; Li, J. An injectable gellan gum-based hydrogel that inhibits Staphylococcus aureus for infected bone defect repair. *J. Mater. Chem. B* **2022**, *10* (2), 282.

(8) Lu, H.; Liu, Y.; Guo, J.; Wu, H.; Wang, J.; Wu, G. Biomaterials with Antibacterial and Osteoinductive Properties to Repair Infected Bone Defects. *Int. J. Mol. Sci.* **2016**, *17* (3), 334 DOI: 10.3390/ijms17030334.

(9) Masters, E. A.; Ricciardi, B. F.; Bentley, K. L. d. M.; Moriarty, T. F.; Schwarz, E. M.; Muthukrishnan, G. Skeletal infections: microbial pathogenesis, immunity and clinical management. *Nature Reviews Microbiology* **2022**, *20* (7), 385.

(10) Gao, X.; Xu, Z.; Li, S.; Cheng, L.; Xu, D.; Li, L.; Chen, L.; Xu, Y.; Liu, Z.; Liu, Y.; Sun, J. Chitosan-vancomycin hydrogel incorporated bone repair scaffold based on staggered orthogonal structure: a viable dually controlled drug delivery system. *RSC Adv.* **2023**, *13* (6), 3759.
(11) Cheng, L.; Xu, Z.; Liu, Y.; Zhou, D.; Sun, M.; Xu, Y.; Chen, L.; Sun, J. 3D-Printed Drug-Loaded Composite Scaffolds to Promote Osteogenesis and Antibacterial Activity. *ACS Applied Polymer Materials* **2022**, *4* (6), 4476.
(12) Zhao, Z.; Vizetto-Duarte, C.; Moay, Z. K.; Setyawati, M. I.; Rakshit, M.; Kathawala, M. H.; Ng, K. W. Composite Hydrogels in Three-Dimensional in vitro Models. *Front. Bioeng. Biotechnol.* **2020**, *8*, 611 DOI: 10.3389/fbioe.2020.00611.
(13) Chen, J.; Chen, J.; Zhu, Z.; Sun, T.; Liu, M.; Lu, L.; Zhou, C.; Luo, B. Drug-Loaded and Anisotropic Wood-Derived Hydrogel Periosteum with Super Antibacterial, Anti-Inflammatory, and Osteogenic Activities. *ACS Appl. Mater. Interfaces* **2022**, *14* (45), 50485.
(14) Ullah, I.; Hussain, Z.; Ullah, S.; Zahra, Q.; Zhang, Y.; Mehmood, S.; Liu, X.; Kamya, E.; Waseem Ghani, M.; Mansoorianfar, M.; Wang, Z.; Wang, Z.; Pei, R. An osteogenic, antibacterial, and anti-inflammatory nanocomposite hydrogel platform to accelerate bone reconstruction. *J. Mater. Chem. B* **2023**, *11* (25), 5830.
(15) Al Maruf, D. S. A.; Ghosh, Y. A.; Xin, H.; Cheng, K.; Mukherjee, P.; Crook, J. M.; Wallace, G. G.; Klein, T. J.; Clark, J. R. Hydrogel: A Potential Material for Bone Tissue Engineering Repairing the Segmental Mandibular Defect. *Polymers* **2022**, *14* (19), 4186 DOI: 10.3390/polym14194186.
(16) Rahmanian-Devin, P.; Baradaran Rahimi, V.; Askari, V. R. Thermosensitive Chitosan-β-Glycerophosphate Hydrogels as Targeted Drug Delivery Systems: An Overview on Preparation and Their Applications. *Adv. Pharmacol. Pharm. Sci.* **2021**, *2021*, No. 6640893.
(17) Peers, S.; Montembault, A.; Ladavière, C. Chitosan hydrogels for sustained drug delivery. *Journal of controlled release: official journal of the Controlled Release Society* **2020**, *326*, 150.
(18) Zuo, R.; Shi, J.; Jiang, S.; Chu, M.; Wang, Q.; Kong, L.; Kang, Q.; Guo, Y.; Guan, J. Promotion of the genipin crosslinked chitosan-fiber hydrogel loaded with sustained release of clemastine fumarate in diabetic wound repair. *Int. J. Biol. Macromol.* **2023**, *226*, 900.
(19) Upadhyaya, L.; Singh, J.; Agarwal, V.; Tewari, R. P. The implications of recent advances in carboxymethyl chitosan based targeted drug delivery and tissue engineering applications. *Journal of controlled release: official journal of the Controlled Release Society* **2014**, *186*, 54.
(20) Geng, Y.; Xue, H.; Zhang, Z.; Panayi, A. C.; Knoedler, S.; Zhou, W.; Mi, B.; Liu, G. Recent advances in carboxymethyl chitosan-based materials for biomedical applications. *Carbohydr. Polym.* **2023**, *305*, No. 120555.
(21) Bayram, C. Carboxymethyl chitosan-glycerol multi-aldehyde based self-healing hydrogel system. *Int. J. Biol. Macromol.* **2023**, *239*, No. 124334.
(22) Khan, M. U. A.; Razak, S. I. A.; Haider, S.; Mannan, H. A.; Hussain, J.; Hasan, A. Sodium alginate-f-GO composite hydrogels for tissue regeneration and antitumor applications. *Int. J. Biol. Macromol.* **2022**, *208*, 475.
(23) Liu, L.; Lu, Y.; Qiu, D.; Wang, D.; Ding, Y.; Wang, G.; Liang, Z.; Shen, Z.; Li, A.; Chen, X.; Song, H. Sodium alginate-derived porous carbon: Self-template carbonization mechanism and application in capacitive energy storage. *J. Colloid Interface Sci.* **2022**, *620*, 284.
(24) Yang, Y.; Xu, Z.; Guo, Y.; Zhang, H.; Qiu, Y.; Li, J.; Ma, D.; Li, Z.; Zhen, P.; Liu, B.; Fan, Z. Novel core-shell CHX/ACP nanoparticles effectively improve the mechanical, antibacterial and remineralized properties of the dental resin composite. *Dental materials: official publication of the Academy of Dental Materials* **2021**, *37* (4), 636.
(25) Zhou, D.; Xu, Z.; Li, Y.; Chen, L.; Liu, Y.; Xu, Y.; Meng, K.; Cheng, L.; Sun, J. Preparation and characterization of thermosensitive hydrogel system for dual sustained-release of chlorhexidine and bovine serum albumin. *Mater. Lett.* **2021**, *300*, No. 130121, DOI: 10.1016/j.matlet.2021.130121.
(26) Cheng, L.; Xu, Z.; Li, Y.; Zhou, D.; Chen, L.; Liu, Y.; Xu, Y.; Meng, K.; Sun, J. Preparation and properties of the inclusion complex of chlorohexidine with β-Cyclodextrin. *Mater. Lett.* **2022**, *309*, No. 131460, DOI: 10.1016/j.matlet.2021.131460.
(27) Inoue, B. S.; Streit, S.; Dos Santos Schneider, A. L.; Meier, M. M. Bioactive bacterial cellulose membrane with prolonged release of chlorhexidine for dental medical application. *Int. J. Biol. Macromol.* **2020**, *148*, 1098.
(28) Wang, Y.; Cao, X.; Ma, M.; Lu, W.; Zhang, B.; Guo, Y. A GelMA-PEGDA-nHA Composite Hydrogel for Bone Tissue Engineering. *Materials* **2020**, *13* (17), 3735 DOI: 10.3390/ma13173735.
(29) Parameswaran-Thankam, A.; Al-Anbaky, Q.; Al-Karakooly, Z.; RanguMagar, A. B.; Chhetri, B. P.; Ali, N.; Ghosh, A. Fabrication and characterization of hydroxypropyl guar-poly (vinyl alcohol)-nano hydroxyapatite composite hydrogels for bone tissue engineering. *Journal of biomaterials science. Polymer edition* **2018**, *29* (17), 2083.
(30) Kavitha Sri, A.; Arthi, C.; Neya, N. R.; Hikku, G. S. Nano-hydroxyapatite/collagen composite as scaffold material for bone regeneration. *Biomed Mater.* **2023**, *18* (3), No. 032002, DOI: 10.1088/1748-605X/acc99e.
(31) Hoveidaei, A. H.; Sadat-Shojai, M.; Mosalamiaghili, S.; Salarikia, S. R.; Roghani-Shahraki, H.; Ghaderpanah, R.; Ersi, M. H.; Conway, J. D. Nano-hydroxyapatite structures for bone regenerative medicine: Cell-material interaction. *Bone* **2024**, *179*, No. 116956.
(32) Mohd Zaffarin, A. S.; Ng, S. F.; Ng, M. H.; Hassan, H.; Alias, E. Nano-Hydroxyapatite as a Delivery System for Promoting Bone Regeneration In Vivo: A Systematic Review. *Nanomaterials* **2021**, *11* (10), 2569 DOI: 10.3390/nano11102569.
(33) Piccirillo, C.; Castro, P. L. M. Calcium hydroxyapatite-based photocatalysts for environment remediation: Characteristics, performances and future perspectives. *J. Environ. Manage.* **2017**, *193*, 79.
(34) Mayer, I.; Cuisinier, F. J.; Gdalya, S.; Popov, I. TEM study of the morphology of Mn2+-doped calcium hydroxyapatite and beta-tricalcium phosphate. *Journal of inorganic biochemistry* **2008**, *102* (2), 311.
(35) Dias, A. M.; do Nascimento Canhas, I.; Bruziquesi, C. G. O.; Speziali, M. G.; Sinisterra, R. D.; Cortés, M. E. Magnesium (Mg2 +), Strontium (Sr2 +), and Zinc (Zn2 +) Co-substituted Bone Cements Based on Nano-hydroxyapatite/Monetite for Bone Regeneration. *Biological trace element research* **2023**, *201* (6), 2963.
(36) Hou, H. H.; Lee, B. S.; Liu, Y. C.; Wang, Y. P.; Kuo, W. T.; Chen, I. H.; He, A. C.; Lai, C. H.; Tung, K. L.; Chen, Y. W. Vapor-Induced Pore-Forming Atmospheric-Plasma-Sprayed Zinc-, Strontium-, and Magnesium-Doped Hydroxyapatite Coatings on Titanium Implants Enhance New Bone Formation-An In Vivo and In Vitro Investigation. *Int. J. Mol. Sci.* **2023**, *24* (5), 4933 DOI: 10.3390/ijms24054933.
(37) Radulescu, D. E.; Vasile, O. R.; Andronescu, E.; Ficai, A. Latest Research of Doped Hydroxyapatite for Bone Tissue Engineering. *Int. J. Mol. Sci.* **2023**, *24* (17), 13157 DOI: 10.3390/ijms241713157.
(38) Liu, J.; Rawlinson, S. C.; Hill, R. G.; Fortune, F. Strontium-substituted bioactive glasses in vitro osteogenic and antibacterial effects. *Dental materials: official publication of the Academy of Dental Materials* **2016**, *32* (3), 412.
(39) Bussola Tovani, C.; Gloter, A.; Azaïs, T.; Selmane, M.; Ramos, A. P.; Nassif, N. Formation of stable strontium-rich amorphous calcium phosphate: Possible effects on bone mineral. *Acta Biomater* **2019**, *92*, 315.
(40) Ding, X.; Li, X.; Li, C.; Qi, M.; Zhang, Z.; Sun, X.; Wang, L.; Zhou, Y. Chitosan/Dextran Hydrogel Constructs Containing Strontium-Doped Hydroxyapatite with Enhanced Osteogenic Potential in Rat Cranium. *ACS biomaterials science & engineering* **2019**, *5* (9), 4574.
(41) Ji, S.; Zhou, S.; Zhang, X.; Chen, W.; Jiang, X. An oxygen-sensitive probe and a hydrogel for optical imaging and photodynamic

antimicrobial chemotherapy of chronic wounds. *Biomaterials Science* **2022**, *10* (8), 2054.
(42) Li, Z.-Y.; Ge, X.; Wang, Q.; Zhou, Z.-H. Strontium Doped Hydroxyapatite Nanoparticles: Synthesis, Characterization and Simulation. *J. Inorg. Mater.* **2020**, *35*, 1283 DOI: 10.15541/jim20190439.
(43) Edwin, N.; Wilson, P. Investigations on sonofragmentation of hydroxyapatite crystals as a function of strontium incorporation. *Ultrasonics sonochemistry* **2019**, *50*, 188.
(44) Douglas, T. E. L.; Łapa, A.; Reczyńska, K.; Krok-Borkowicz, M.; Pietryga, K.; Samal, S. K.; Declercq, H. A.; Schaubroeck, D.; Boone, M.; Van der Voort, P.; De Schamphelaere, K.; Stevens, C. V.; Bliznuk, V.; Balcaen, L.; Parakhonskiy, B. V.; Vanhaecke, F.; Cnudde, V.; Pamuła, E.; Skirtach, A. G. Novel injectable, self-gelling hydrogel–microparticle composites for bone regeneration consisting of gellan gum and calcium and magnesium carbonate microparticles. *Biomed. Mater.* **2016**, *11* (6), No. 065011, DOI: 10.1088/1748-6041/11/6/065011.
(45) Ren, B.; Chen, X.; Du, S.; Ma, Y.; Chen, H.; Yuan, G.; Li, J.; Xiong, D.; Tan, H.; Ling, Z.; Chen, Y.; Hu, X.; Niu, X. Injectable polysaccharide hydrogel embedded with hydroxyapatite and calcium carbonate for drug delivery and bone tissue engineering. *Int. J. Biol. Macromol.* **2018**, *118*, 1257.
(46) Khan, M. U. A.; Stojanović, G. M.; Hassan, R.; Anand, T. J. S.; Al-Ejji, M.; Hasan, A. Role of Graphene Oxide in Bacterial Cellulose-Gelatin Hydrogels for Wound Dressing Applications. *ACS omega* **2023**, *8* (18), 15909.
(47) Zhou, X.; Sun, J.; Wo, K.; Wei, H.; Lei, H.; Zhang, J.; Lu, X.; Mei, F.; Tang, Q.; Wang, Y.; Luo, Z.; Fan, L.; Chu, Y.; Chen, L. nHA-loaded gelatin/alginate hydrogel with combined physical and bioactive features for maxillofacial bone repair. *Carbohydr. Polym.* **2022**, *298*, No. 120127.
(48) Zhang, L.; Dong, Y.; Liu, Y.; Liu, X.; Wang, Z.; Wan, J.; Yu, X.; Wang, S. Multifunctional hydrogel/platelet-rich fibrin/nanofibers scaffolds with cell barrier and osteogenesis for guided tissue regeneration/guided bone regeneration applications. *Int. J. Biol. Macromol.* **2023**, *253* (Part 4), No. 126960.
(49) Zhao, W.; Li, Y.; Zhou, A.; Chen, X.; Li, K.; Chen, S.; Qiao, B.; Jiang, D. Controlled release of basic fibroblast growth factor from a peptide biomaterial for bone regeneration. *Royal Society open science* **2020**, *7* (4), No. 191830.
(50) Chen, Y.; Zhou, Y.; Yang, S.; Li, J. J.; Li, X.; Ma, Y.; Hou, Y.; Jiang, N.; Xu, C.; Zhang, S.; Zeng, R.; Tu, M.; Yu, B. Novel bone substitute composed of chitosan and strontium-doped α-calcium sulfate hemihydrate: Fabrication, characterisation and evaluation of biocompatibility. *Materials science & engineering. C, Materials for biological applications* **2016**, *66*, 84.
(51) Xu, L.; Ye, Q.; Xie, J.; Yang, J.; Jiang, W.; Yuan, H.; Li, J. An injectable gellan gum-based hydrogel that inhibits Staphylococcus aureus for infected bone defect repair. *Journal of materials chemistry. B* **2022**, *10* (2), 282.
(52) Xue, X.; Hu, Y.; Wang, S.; Chen, X.; Jiang, Y.; Su, J. Fabrication of physical and chemical crosslinked hydrogels for bone tissue engineering. *Bioactive materials* **2022**, *12*, 327.
(53) Feng, P.; Wu, P.; Gao, C.; Yang, Y.; Guo, W.; Yang, W.; Shuai, C. A Multimaterial Scaffold With Tunable Properties: Toward Bone Tissue Repair. *Adv. Sci.* **2018**, *5* (6), No. 1700817.
(54) Caverzasio, J. Strontium ranelate promotes osteoblastic cell replication through at least two different mechanisms. *Bone* **2008**, *42* (6), 1131.
(55) Tian, Q.; Lin, J.; Rivera-Castaneda, L.; Tsanhani, A.; Dunn, Z. S.; Rodriguez, A.; Aslani, A.; Liu, H. Nano-to-Submicron Hydroxyapatite Coatings for Magnesium-based Bioresorbable Implants - Deposition, Characterization, Degradation, Mechanical Properties, and Cytocompatibility. *Sci. Rep.* **2019**, *9* (1), 810.

https://doi.org/10.1021/acsomega.4c01237
ACS Omega 2024, 9, 22230−22239